

# Anisotropic emission of thermal dielectrons from Au+Au collisions at $\sqrt{s_{NN}} = 200$ GeV with EPOS3

Sheng-Xu Liu,<sup>1</sup> Fu-Ming Liu,<sup>1</sup> Klaus Werner,<sup>2</sup> and Meng Yue<sup>1</sup>

<sup>1</sup>*Institute of Particle Physics and Key laboratory of Quark & Lepton Physics (Ministry of Education), Central China Normal University, Wuhan, China*

<sup>2</sup>*Laboratoire SUBATECH, University of Nantes - IN2P3/CNRS - Ecole des Mines, Nantes, France*  
(Dated: November 26, 2021)

Dileptons, as an electromagnetic probe, are crucial to study the properties of a Quark-Gluon Plasma (QGP) created in heavy ion collisions. We calculated the invariant mass spectra and the anisotropic emission of thermal dielectrons from Au+Au collisions at the Relativistic Heavy Ion Collider (RHIC) energy  $\sqrt{s_{NN}} = 200$  GeV based on EPOS3. This approach provides a realistic (3+1)-dimensional event-by-event viscous hydrodynamic description of the expanding hot and dense matter with a very particular initial condition, and a large set of hadron data and direct photons (besides  $v_2$  and  $v_3$  !) can be successfully reproduced. Thermal dilepton emission from both the QGP phase and the hadronic gas are considered, with the emission rates based on Lattice QCD and a vector meson model, respectively. We find that the computed invariant mass spectra (thermal contribution + STAR cocktail) can reproduce the measured ones from STAR at different centralities. Different compared to other model predictions, the obtained elliptic flow of thermal dileptons is larger than the STAR measurement referring to all dileptons. We observe a clear centrality dependence of thermal dilepton not only for elliptic flow  $v_2$  but also for higher orders. At a given centrality,  $v_n$  of thermal dileptons decreases monotonically with  $n$  for  $2 \leq n \leq 5$ .

PACS numbers:

## I. INTRODUCTION

Dielectron spectra have been measured by the PHENIX Collaboration [1] and the STAR Collaboration [2] in Au+Au collisions at  $\sqrt{s_{NN}} = 200$  GeV at Relativistic Heavy Ion Collider (RHIC). In fact, dileptons have been proposed as a kind of clear probe in the study of the hot and dense matter named Quark-Gluon Plasma (QGP), created in heavy ion collisions [3], due to the fact that dileptons do not interact strongly and therefore survive the whole evolution of a heavy ion collisions. This concerns the initial hard scattering Drell-Yan pairs, the thermal emission from the QGP and the Hadron Gas phase, and the decay of light and heavy flavor hadrons. The dielectron spectra from both STAR and PHENIX show the low mass enhancement beyond the cocktail. This phenomenon was also observed in the CERES dielectron [4, 5] and NA60 dimuon data [6]. Medium modifications of the  $\rho$  meson spectral functions have been considered to describe this enhancement, based on hadronic many body effective theories [7–9] and using a relatively simple expanding fireball model. Another approach used the forward scattering amplitude method [10, 11] and viscous hydrodynamics with smooth initial conditions as medium. These two methods could get a similar result [12]. The combination of these two methods [13] could also describe the STAR dielectrons data reasonably well, using a 2+1 dimensional ideal hydrodynamic model. In addition, a microscopic transport model- Parton-Hadron String Dynamics (PHSD) [14–16] has successfully described the observed dimuon enhancement by NA60 and dielectron enhancement by STAR.

Elliptic flow is the second Fourier coefficient of the az-

imuthal particle distribution. The thermal elliptic flows of dileptons has been studied in hydrodynamic simulations with smooth initial conditions [17, 18] and also with fluctuating initial conditions [19]. The fluctuations seem to play an important role in elliptic flows of dileptons in heavy ion collisions. However, the predicted elliptic flows of thermal dileptons are small, so do their predicted elliptic flows of direct photons. The observed large elliptic flow of direct photons seems a big puzzle in our field. Using EPOS3102, a (3+1)D viscous hydrodynamic model well constrained by hadron data, it seems that one can reproduce naturally the measured elliptic and trianger flow of direct photons[20]. In this paper we will compute thermal dilepton production in an approach which has been successfully tested concerning hadron and photon production. This will serve as a benchmark to a systematic compilation of hadron, dilepton and photon results.

In additional to the thermal sources, dileptons may be produced from non-thermal sources such as primordial Drell-Yan annihilation and electromagnetic final-state decays of long-lived hadrons. To account for these, STAR cocktail results from Refs [2] have been employed in this paper.

The paper is organized as following. In section 2, we briefly review the calculation approach of thermal dilepton emission rates from quark-gluon plasma (QGP) and hadronic matter. In section 3, the results will be presented. Finally, a conclusion is made in section 4.

## II. CALCULATION APPROACH

The calculation of dilepton production is obtained as an integration over an emission rate  $\frac{dR}{d^4q} = \frac{dN_{ll}}{d^4x d^4q}$ , based on the space-time evolution of a QGP and the hadronic stage according to EPOS3[21]. We use a QGP emission rate from extrapolating lattice QCD results to finite momenta. The calculation of the hadronic emission rate is done by employing the vector meson dominance model. We consider explicitly the  $\rho$  meson, for the rest we refer to the so-called cocktail according to the STAR experiment (dileptons from decays of measured resonances) [22]. This procedure to compute dileptons, discussed in more detail in the following, will be referred to as EPOS3+DiL1.

### A. The EPOS3 dynamics

As explained in [21], EPOS3 is an event generator based on a 3+1D viscous hydrodynamical evolution starting from flux tube initial conditions, which are generated in the Gribov-Regge multiple scattering framework [23]. An individual scattering is referred to as Pomeron, identified with a parton ladder, eventually showing up as flux tubes (or strings). Each parton ladder is composed of a pQCD hard process, plus initial and final state linear parton emission. Nonlinear effects are considered by using saturation scales  $Q_s$ , depending on the energy and the number of participants connected to the Pomeron in question.

The final state partonic system (corresponding to a Pomeron) amounts to (usually two) color flux tubes, being mainly longitudinal, with transversely moving pieces carrying the  $p_t$  of the partons from hard scatterings [23, 24]. One has two flux tubes, based on the cylindrical topology of the Pomerons, but each quark-antiquark pair in the parton ladder will cut a string into two, in this sense one may have more than two flux tubes. In any case, these flux tubes constitute eventually both bulk matter, also referred to as ‘‘core’’ [25] (which thermalizes, flows, and finally hadronizes) and jets (also referred to as ‘‘corona’’), according to some criteria based on the energy of the string segments and the local string density.

Concerning the core, we use a 3+1D viscous hydrodynamic approach, employing a realistic equation of state, compatible with lQCD results. We employ for all calculations in this paper a value of  $\eta/S = 0.08$ . Whenever a temperature of  $T_H = 168$  MeV is reached, we apply the usual Cooper-Frye procedure to convert the fluid into particles. From this point on, we apply a hadronic cascade [26], based on hadronic cross sections.

So we have two phases, a plasma phase with a hydrodynamical expansion, and a hadronic phase, with individual hadron-hadron collisions. From the fluid dynamical expansion of the plasma, we get the complete space-time information, i.e. the collective velocity  $\vec{v}(x)$  (which define the local rest frame (LRF) at each point  $x$ ) and the

temperature  $T(x)$  of matter for a given space-time  $x$ , starting from some initial proper time  $\tau_0$ . This is the basis of the dilepton (rate) calculations discussed later. In the hadronic phase, we have from EPOS a complete description of hadron trajectories. We may use this to compute energy densities, flow velocities and net baryon density. Assuming that the system may be approximated by a resonance gas in equilibrium, we use the corresponding equation of state, c.f. Appendix C of [27], to get the temperature  $T$  and baryon chemical potential  $\mu_B$  at any point in space time. This will be used for the dilepton rate calculations.

### B. Invariant mass spectrum

The invariant mass spectrum of thermal dileptons is calculated as an integration of the dilepton emission rates over the realistic space-time evolution of the heavy-ion collision system and the momentum space of the dileptons [7], namely,

$$\frac{dN_{ll}}{dM}(M) = \int d^4x \frac{M d^3q}{q_0} \frac{dN_{ll}}{d^4x d^4q}(T(x), q^*). \quad (1)$$

Here,  $M$  and  $q$  are the invariant mass and four momentum of the dilepton pair, satisfying  $M^2 = q^2$ . The four momentum  $q^*$  of the dilepton pair as viewed from local rest frame is given as

$$q_0^* = \gamma q_0 - \gamma \vec{q} \cdot \vec{v} \quad (2)$$

and

$$\vec{q}^* = \vec{q} + (\gamma - 1)(\vec{q} \cdot \vec{v}) \cdot \vec{v}/v^2 - \gamma q^0 \vec{v}, \quad (3)$$

where  $\vec{v}$  is the flow velocity,  $v^2 = \vec{v} \cdot \vec{v}$  and  $\gamma = 1/\sqrt{1 - v^2/c^2}$ . The flow velocity  $\vec{v}(x)$  and the temperature  $T(x)$  at each space-time point  $x$  are provided by the above-mentioned EPOS3 dynamics. The momentum integral ranges from 0 to 5GeV/c (results do not depend on the upper bound as long as it is much bigger than the temperature). The quantity  $d^4x = \tau d\tau dx dy d\eta$  is the space-time element.

The space-time integral starts from the initial time  $\tau_0$  of the hydrodynamical evolution up to the end of hadron cascade. In the hadronic phase, uRQMD has been employed after freeze-out in EPOS, and macroscopic quantities such as energy-momentum and flow velocity are reconstructed in order to calculate thermal emissions of dileptons and photons, as mentioned earlier. The emission rate is the number of dileptons emitted per space-time unit and per energy-momentum unit. Thermal dileptons emitted from both the QGP phase and the hadron gas phase are considered, as explained in the following.

### C. Dilepton Emission Rate in the Quark-Gluon Plasma

For dileptons emitted from the QGP phase, asymptotic freedom implies that the production rate in the intermediate invariant mass region ( $1. < M < 3.0\text{GeV}/c^2$ ) at high temperatures and densities can be described by perturbation theory as in Ref.[7]. Recent progress using thermal lattice QCD (lQCD) to calculate dilepton rates nonperturbatively at vanishing three-momentum  $q = 0$  has been reported in Ref. [28]. For practical applications, an extrapolation to finite  $q$  values is needed. A construction proposed in Ref. [9] and employed in our calculation reads

$$\frac{d^4R}{d^4q} = \frac{\alpha^2}{4\pi^4} f^B(q_0, T) C_{\text{EM}} \left\{ 1 + \frac{2T}{q} \ln \left[ \frac{1+x_+}{1+x_-} \right] + 2\pi\alpha_s \frac{T^2}{M^2} K F(M^2) \ln \left( 1 + \frac{2.912q_0}{4\pi\alpha_s T} \frac{2q_0^2 + M^2}{3q_0^2} \right) \right\}, \quad (4)$$

where  $\alpha$  is the electromagnetic coupling constant,  $f^B(q_0, T)$  the thermal Bose distribution,  $C_{\text{EM}} \equiv \sum_{q=u,d,s} e_q^2$ ,  $x_{\pm} = \exp[-(q_0 \pm q)/2T]$ . The quantity  $\alpha_s$  is the temperature-dependent strong coupling constant,  $K$  a constant factor (equal 2), and finally we have a form factor  $F(M^2) = \frac{\Lambda^2}{\Lambda^2 + M^2}$  with  $\Lambda = 2T$ .

### D. Rates from hadronic medium

According to the vector meson dominance model [29], the hadronic electromagnetic current operator is equal to the linear combination of the known neutral vector meson field operators, most notably  $V=\rho, \omega, \phi$ . This describes dilepton production successfully [7], where the dilepton emission rate via the vector meson  $V$  is [11]

$$\frac{d^4R_V}{d^4q} = -\frac{\alpha^2 m_V^4}{\pi^3 M^2 g_V^2} \text{Im} D_V \frac{1}{e^{\frac{q_0}{T}} - 1}, \quad (5)$$

with the coupling constant  $g_V$  determined by the measured decay rate of vector-meson to dilepton production in vacuum, and  $m_V$  being the mass of the vector-meson. The imaginary part of the retarded vector meson propagator is given as

$$\text{Im} D_V = \frac{\text{Im} \Pi_V}{(M^2 - m_V^2 - \text{Re} \Pi_V)^2 + (\text{Im} \Pi_V)^2}, \quad (6)$$

where  $\Pi_V$  is the self-energy of the vector meson  $V$ .

We consider  $V=\rho$  and neglect the complexity of  $\omega$  and  $\phi$ , which seems consistent with the STAR dilepton data taking[2]. The  $\rho$  meson self-energy

$$\Pi_\rho = \Pi_\rho^{\text{vac}} + \sum_a \Pi_{\rho a}, \quad (7)$$

for the contribution from the vacuum and from  $\rho$  meson scattering with hadrons of type  $a$  in the hadronic gas, respectively.

The vacuum part  $\Pi_\rho^{\text{vac}}$  is obtained from Gounaris-Sakurai formula as Refs [29, 30], which could describe the pion electromagnetic form factor well, as measured in  $e^+e^-$  annihilation Refs [31]:

$$\text{Re} \Pi_\rho^{\text{vac}} = \frac{g_\rho^2 M^2}{48\pi^2} \left[ \left( 1 - \frac{4m_\pi^2}{M^2} \right)^{\frac{3}{2}} \ln \left| \frac{1 + \sqrt{1 - \frac{4m_\pi^2}{M^2}}}{1 - \sqrt{1 - \frac{4m_\pi^2}{M^2}}} \right| + 8m_\pi^2 \left( \frac{1}{M^2} - \frac{1}{m_\rho^2} \right) - 2 \left( \frac{p_0}{\omega_0} \right)^3 \ln \left( \frac{\omega_0 + p_0}{m_\pi} \right) \right], \quad (8)$$

$$\text{Im} \Pi_\rho^{\text{vac}} = -\frac{g_\rho^2 M^2}{48\pi} \left( 1 - \frac{4m_\pi^2}{M^2} \right)^{\frac{3}{2}}. \quad (9)$$

Here,  $2\omega_0 = m_\rho = 2\sqrt{m_\pi^2 + p_0^2}$ . The vacuum width is  $\Gamma_\rho^{\text{vac}} = \frac{g_\rho^2}{48\pi} m_\rho \left( \frac{p_0}{\omega_0} \right)^3$ .

The interactive part  $\Pi_{\rho a}(E, p)$  is obtained from  $\rho$  scattering from hadron of type  $a$  in the hadronic gas

$$\Pi_{\rho a}(E, p) = -4\pi \int \frac{d^3k}{(2\pi)^3} n_a(\omega) \frac{\sqrt{s}}{\omega} f_{\rho a}^{\text{c.m.}}(s), \quad (10)$$

where  $f^{\text{c.m.}}$  is the forward scattering amplitude in the c.m. system,  $E$  and  $p$  are the energy and momentum of the  $\rho$  meson,  $\omega^2 = m_a^2 + k^2$ . The most copious hadrons in the hadronic gas such as  $\pi$  mesons ( $a = \pi$ ) and nucleons ( $a = N$ ) are considered in our calculation. The quantity  $n_a$  is the Bose-Einstein occupation number of  $\pi$  mesons and the Fermi-Dirac occupation number for nucleons, with temperature  $T$  and baryon chemical potential  $\mu_B$  of the thermal bath provided by EPOS3 mentioned above. According to Eq.(2-3), the emitted dileptons will get a Lorentz boost with the collective flow velocity offered by EPOS3, so the interactive term of self-energy and the resulted emission rate are calculated in the rest frame of the thermal bath.

The  $\rho a$  forward scattering amplitude in the center-of-mass frame could be written as

$$f_{\rho a}^{\text{c.m.}} = (1-x)f_{\text{Res}} + x f_{\text{Reg}} + f_{\text{Pom}}, \quad (11)$$

where the Pomeron term is dual to the background upon which the resonances are superimposed,  $x$  is a function that matches the low energy Breit-Wigner resonances and high energy Reggions (dual to s-channel resonances) smoothly:

$$x = 0.5 \left( 1 + \tanh \left( \frac{E_\rho - m_\rho - E_\Delta}{0.3} \right) \right), \quad (12)$$

where  $E_\Delta$  is 1GeV and 4GeV for  $\rho\pi$  and  $\rho N$  scattering, respectively[13].

Regge and Pomeron term have the same form [10]:

$$f_{\text{Reg/Pom}} = -\frac{q_{\text{c.m.}}}{4\pi s} \frac{1 + e^{-i\pi\alpha}}{\sin \pi\alpha} s^\alpha r^{\rho a}, \quad (13)$$

where the intercept  $\alpha$  and residue  $r^{\rho N}$ ,  $r^{\rho\pi}$  are 0.642, 28.59, 12.74 for Regges and 1.093, 11.88, 7.508 for

Pomerons, respectively (the units yield a cross section in mb with energy in GeV) .

The resonance term is [10]:

$$f_{\text{Res}} = \frac{1}{2q_{c.m.}} \sum_R W_{\rho a}^R \frac{\Gamma_{R \rightarrow \rho a}}{M_R - \sqrt{s} - \frac{1}{2}i\Gamma_R}, \quad (14)$$

which involves a sum over a series of Breit-Wigner resonances of mass  $M_R$  and total width  $\Gamma_R$ . The resonances R used in our calculation are listed in table I for  $a = \pi$  and table II for  $a = N$ , with R's name, mass, decay width, branching ratio, spin, isospin and relative angular momentum Ref. [10, 13].

Table I: Meson resonances  $R$  for  $\rho\pi$  processes.

Name(R)	Mass( $M_R$ )	$\Gamma$	BR	S	IS	L
$\phi(1020)$	1.020	0.0045	0.13	1	0	1
$h_1(1170)$	1.170	0.36	1	1	0	0
$a_1(1260)$	1.230	0.40	0.68	1	1	0
$\pi(1300)$	1.300	0.40	0.32	0	1	1
$a_2(1320)$	1.318	0.107	0.70	2	1	2
$\omega(1420)$	1.419	0.174	1	1	0	1

Table II: Baryon resonances  $R$  for  $\rho N$  processes.

Name(R)	Mass( $M_R$ )	$\Gamma$	BR	S	IS	L
N(2090)	1.928	0.414	0.49	0.5	0.5	0
N(1700)	1.737	0.249	0.13	1.5	0.5	0
N(2080)	1.804	0.447	0.26	1.5	0.5	0
N(2190)	2.127	0.547	0.29	3.5	0.5	2
N(2100)	1.885	0.113	0.27	0.5	0.5	1
N(1720)	1.717	0.383	0.87	1.5	0.5	1
N(1900)	1.879	0.498	0.44	1.5	0.5	1
N(2000)	1.903	0.494	0.60	2.5	0.5	1
$\Delta(1900)$	1.920	0.263	0.38	0.5	1.5	0
$\Delta(1700)$	1.762	0.599	0.08	1.5	1.5	0
$\Delta(1940)$	2.057	0.460	0.35	1.5	1.5	0
$\Delta(2000)$	1.752	0.251	0.22	2.5	1.5	1
$\Delta(1905)$	1.881	0.327	0.86	2.5	1.5	1
N(1520)	1.520	0.124	0.008	1.5	0.5	0
$\Delta(1232)$	1.232	0.118	0.006	1.5	1.5	1

The c.m. amplitude  $f^{c.m.}$  and the scattering amplitude in the rest frame of  $a$ ,  $f_{\rho a}$ , are related by

$$\sqrt{s} f_{\rho a}^{c.m.}(s) = m_a f_{\rho a}(E_\rho), \quad (15)$$

with  $s = m_\rho^2 + m_a^2 + 2E_\rho m_a$ . The latter is plotted in Fig.1 and Fig.2, for  $\rho\pi$  and  $\rho N$  scattering, respectively. The total contribution (Resonances + Pomeron background + Regge) in both are shown as black solid lines, and both are consistent with Ref. [10]. Each individual process  $\rho\pi \rightarrow R$  is also shown in Fig.1. Their sum is shown as

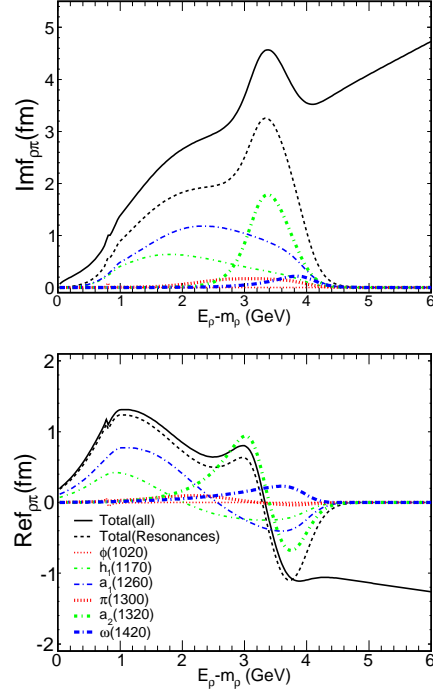


Figure 1: (Color Online) The individual and total amplitude for  $\rho\pi \rightarrow R$  scattering (imaginary part: upper panel, real part: lower panel).

black dashed line. We can see that the contribution of resonances dominates the low energy scattering, and the dominant channels are  $R = a_1(1260)$  and  $h_1(1170)$  due to their large branch ratios. In Fig.2, the relevant individual channels  $\rho N \rightarrow R$  are shown. The black dashed line is the total baryon resonances contribution, among which  $R = \Delta(1905)$ ,  $N(2000)$  and  $N(1720)$  dominate both the imaginary and the real part of the the amplitude for  $\rho N$  scattering.

Putting the forward scattering amplitudes together, we get the interactive term of self-energy of  $\rho$ -meson. The imaginary and real parts are shown in Fig.3, for a fixed  $\rho$ -meson three-momentum  $q = 0.3$  GeV/c at  $T = 150$  MeV, with  $\rho\pi$  scattering dashed lines and  $\rho N$  scattering dotted lines, respectively. The contribution from vacuum is plotted as solid lines. The total one is plotted as dashed-dotted lines. The vacuum contributes when  $M > 2m_\pi$ , then dominates over a wide region. The in-medium effect from interactive term seems rather small.

Yet, the interaction with the medium gives a broadening effect to the spectral density,  $\rho(q) = -\text{Im}D_\rho(q)/\pi$ . In Fig.4,  $\text{Im}D_\rho$  is plotted as a function of invariant mass  $M$  for a  $\rho$ -meson momentum of  $q = 0.3$  GeV/c, in a thermal hadronic gas of temperature  $T=100, 150$  and  $200$  MeV, respectively. The vacuum contribution by itself is plotted as a red solid line. With the increase of medium tempera-

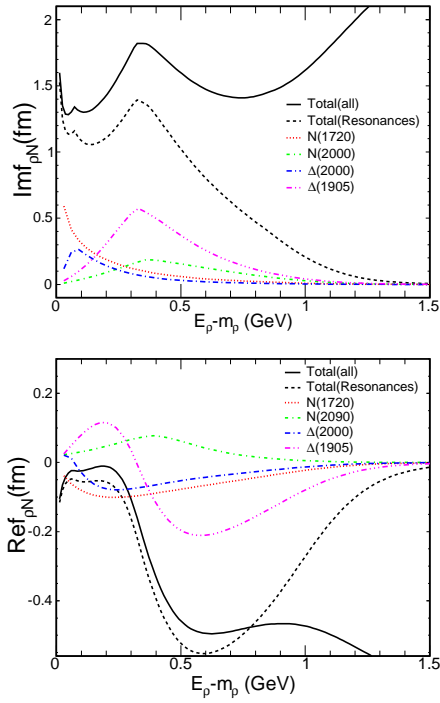


Figure 2: (Color Online) The relevant individual and total amplitude for  $\rho N \rightarrow R$  scattering (imaginary part: upper panel, real part: lower panel) .

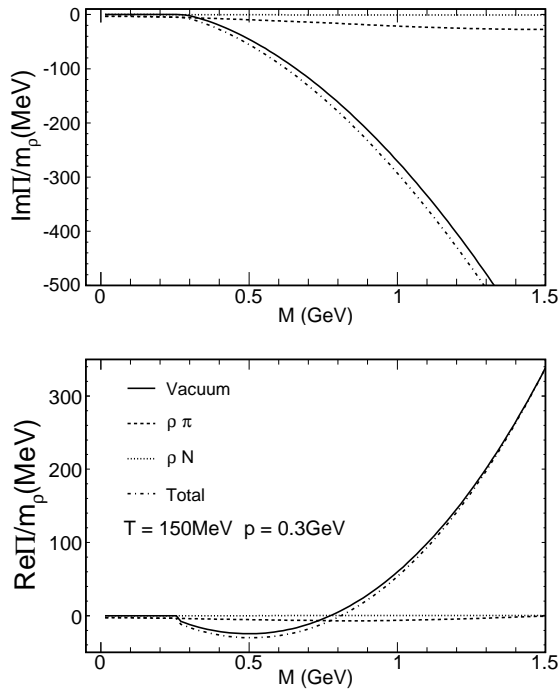


Figure 3: The self-energy of  $\rho$ -meson .

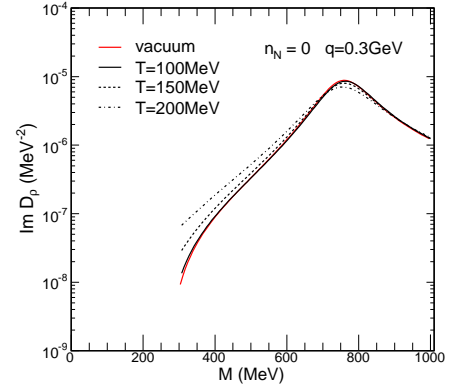


Figure 4: (Color Online) The imaginary part of the  $\rho$  meson propagators as a function of invariant mass for a momentum of  $300 \text{ MeV}/c$  and a nucleon density of  $n_N = 0$ . Results are shown for vacuum (red solid line) and three temperatures,  $T = 100 \text{ MeV}/c$  (black solid line),  $T = 150 \text{ MeV}/c$  (black dashed line),  $T = 200 \text{ MeV}/c$  (black dashed-dotted line).

ture, the  $\rho$ -meson scattering with hadron  $a$  in the medium broadens the spectral density more and more, but the peak remains close to  $\rho$ -meson mass. (Note:  $T=200 \text{ MeV}$  is only to visualize the broadening effect, though it is too high for hadronic gas. )

The emission rates at different phases are now obtained via Eq.(4-5). In Fig.5, the emission rate from the QGP phase is plotted as red thin lines (dotted:  $200 \text{ MeV}$ , solid:  $150 \text{ MeV}$ ), from the HG phase as green thick lines (dotted:  $150 \text{ MeV}$ , solid:  $100 \text{ MeV}$ ). A higher temperature makes a stronger di-electron emission. Nevertheless the HG phase provides a pronounced peak around the  $\rho$ -meson mass  $775 \text{ MeV}$  which exceeds the QGP contribution. This peak is essentially due to the vacuum term in the self-energy (black dashed line). The emission rate from HG phase at  $150 \text{ MeV}$  obtained from effective interaction Lagrangians [32] is also shown as a blue dotted dashed line. It is interesting to see the two rates are quite close to each other, though different approaches and channels are considered.

We should mention here that the above-mentioned emission rates work typically for ideal hydrodynamics. For viscous hydrodynamics such as EPOS3, a viscous correction is needed. The effect of shear viscosity to the spectra and elliptic flow of dileptons in QGP phase and HG phase has been investigated [33]. Similar work has been done for direct photons [34]. The elliptic flow of dileptons seems more sensitive to viscous effect than their spectra, however, it remains a modest effect.

### E. Elliptic flow $v_2$ and Triangular flow $v_3$

The elliptic flow  $v_2$  and the triangular one  $v_3$  of thermal dielectrons are calculated in a similar way as in Refs [35]. The azimuthal angle dependence of the invariant mass spectrum of dielectrons for a given event can be

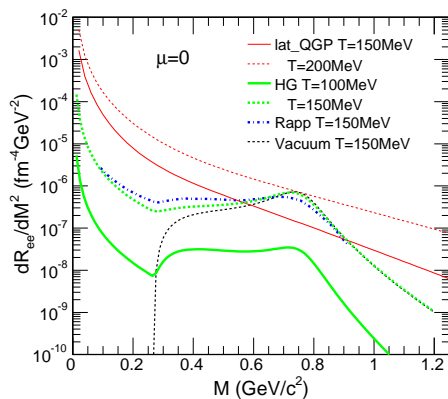


Figure 5: (Color Online) Emission rates of dielectrons from QGP phase (red thin lines) at temperature: 150MeV (solid line), 200MeV (dashed line), and HG phase (green thick lines) at temperature: 100MeV (solid line), 150MeV (dashed line). The vacuum contribution to HG rate at 150MeV is shown as black dashed line. HG rate from effective interaction Lagrangians [32] at 150MeV is shown as blue dashed-dotted line.

decomposed into harmonics of the azimuthal angle  $\phi$  as

$$\frac{dN}{d\phi} \sim \frac{1}{2\pi} [1 + 2v_2 \cos 2(\phi - \psi_2) + 2v_3 \cos 3(\phi - \psi_3) + \dots], \quad (16)$$

where  $v_2(v_n)$  is the elliptic flow (higher order harmonics), and  $\psi_n$  is the  $n$ th-order event plane angle. Obviously,  $v_n$  and  $\psi_n$  depend on the dielectron's invariant mass  $M$  and vary event by event. From Eq. (16), one can easily get

$$v_{e,n} \cos(n\psi_{e,n}) = \frac{\int_0^{2\pi} \cos(n\phi) \frac{dN}{d\phi} |_e d\phi}{\int_0^{2\pi} \frac{dN}{d\phi} |_e d\phi} \quad (17)$$

$$v_{e,n} \sin(n\psi_{e,n}) = \frac{\int_0^{2\pi} \sin(n\phi) \frac{dN}{d\phi} |_e d\phi}{\int_0^{2\pi} \frac{dN}{d\phi} |_e d\phi}, \quad (18)$$

with the subscript  $e$  added to emphasis variables for a single event. Let's note their right sides as  $\langle \cos n\phi \rangle_e$  and  $\langle \sin n\phi \rangle_e$ , respectively. Then, for each event, the harmonics and reaction plane of order  $n$  can be obtained as

$$v_{e,n} = \sqrt{\langle \cos(n\phi) \rangle_e^2 + \langle \sin(n\phi) \rangle_e^2} \quad (19)$$

and

$$\psi_{e,n} = \frac{1}{n} \arctan \frac{\langle \sin(n\phi) \rangle_e}{\langle \cos(n\phi) \rangle_e}. \quad (20)$$

The elliptic flow  $v_2$  and higher order harmonics  $v_n$  of the sample is obtained via event average

$$v_n = \sum_{e=1}^N \frac{v_{e,n}}{N}. \quad (21)$$

This is equivalent to the definition in [36].

### III. RESULTS

The results of thermal dielectrons calculated based on EPOS with initial time  $\tau_0 = 0.35 fm/c$  will be shown in the following.

In Fig.6 is shown the invariant mass spectrum (left panel) and elliptic flow (right panel) of thermal dielectrons at rapidity  $y = 0$  from AuAu collisions at  $\sqrt{s_{NN}} = 200$  GeV with centrality 10-40%. The thermal results (black solid lines) have been decomposed into two contributions, coming from the QGP phase (red dotted lines) and the hadronic phase (blue dashed lines).

From the left plot of Fig.6, it is clear that the QGP contribution dominates the thermal spectra at  $M > 1 GeV/c^2$  region, as in the above figure on emission rates. And the peak from the contribution of the hadronic phase indeed remains around the  $\rho$  mass after the space-time integral of the emission rate. Thus, in the total thermal spectrum, a pronounced peak still exists.

On the right panel of Fig.6, the elliptic flow of dileptons from the QGP phase (dotted line) and from the HG (dashed line) are shown. The elliptic flow of the latter phase is much larger due to a longer development of radial flow. The result of thermal dileptons (solid line), the average of the two flows weighted by their yields in each phase, ranges between the upper bound (values in hadronic phase) and lower bound (values in QGP phase), and is close to the corresponding bound of the dominating phase. Therefore, no evident peak for the elliptic flows of dileptons from either phase still produces a peak of thermal dileptons around the  $\rho$ -meson mass.

A similar phase competition in the invariant mass spectrum and  $v_2$  occurs at other collision centralities, ie, 0-10% and 40-80%.

After investigating the thermal contribution, we would like to compare with data. Thus a study of non-thermal contribution is needed. EPOS3 is almost ready for this goal. For this moment, the employment of STAR cocktail data can also make an independent check of the thermal emission. STAR cocktail contribution includes all the non-thermal contributions, such as contributions from Drell-Yan process and decay of long lived hadrons, such as light mesons, D-mesons and so on. Based on the measurement of those hadrons, Tsallis fitting and decay simulation, STAR offers the invariant mass spectra of the cocktail contribution [22].

In Fig.7, we show the EPOS3+DiL1 thermal contribution (dotted line) and the STAR cocktail (dashed line) from 0-10% Au+Au central collisions at  $\sqrt{s_{NN}} = 200$  GeV. Their sum as the invariant mass spectrum of dielectrons (solid line) is also compared to STAR data [2] (empty dots).

In Fig.8(left panel) the invariant mass spectra of dielectrons from Au+Au collisions at  $\sqrt{s_{NN}} = 200$  GeV for different centralities from EPOS3+DiL1 are compared to STAR data [2, 37], from top to bottom: 0-10% (central), 10-40%, 40-80%, and 0-80% (MinBias). For better visibility, the latter three results are multiplied by factors:

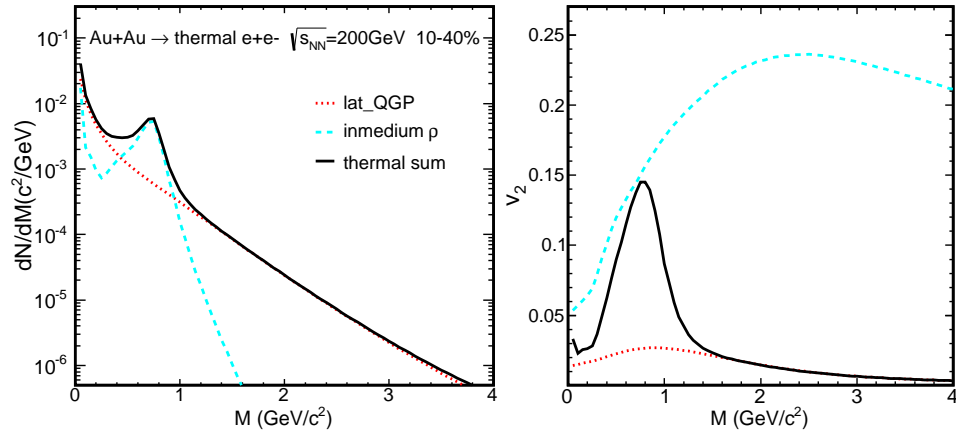


Figure 6: (Color Online) Thermal di-electrons (black solid lines) from AuAu collisions at  $\sqrt{s_{NN}}=200$  GeV with centrality 10-40% are decomposed into di-electrons from QGP phase (red dotted lines) and hadronic phase (blue dashed lines). Left panel: the invariant mass spectra. Right panel: the elliptic flow. All calculations are based on EPOS3+DiL1.

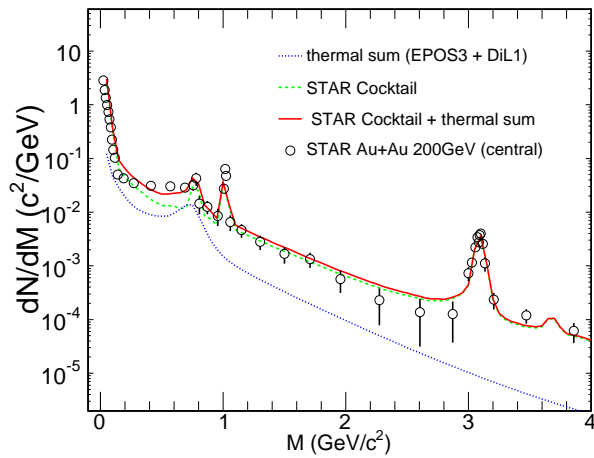


Figure 7: (Color Online) Invariant mass spectra of dielectrons from Au+Au collisions at  $\sqrt{s_{NN}} = 200$  GeV for centrality 0-10%. The STAR data [2] (empty dots) are compared to the total contribution (solid line), which is the sum of the EPOS3+DiL1 thermal contribution (dotted line) and STAR cocktail (dashed line).

0.05, 0.02, 0.0002, respectively. The right panel shows the ratios of measured data and our calculations to the cocktail at different centralities. This precise comparison shows a deviation from the experimental data in low mass region for the first centrality. The calculated results describe the data well for centralities of 10-40% and 40-80% better than 0-10%.

In Fig.9, the red solid line is our calculated elliptic flow of thermal di-electrons from Au+Au minimum bias collisions (0-80% centrality) at  $\sqrt{s_{NN}} = 200$  GeV. As a reference, we also show STAR data [38] (stars) of the elliptic flow of di-electrons (from all sources, of course). The calculated elliptic flow of thermal dielectrons is com-

parable, in fact even larger than data for all di-electrons. The cocktail contribution will inherit a certain elliptic flow because hadrons carry elliptic flow before decaying into di-electrons. Most models predict it to be lower than the STAR reference [9, 11, 19], whereas our result based on EPOS3 is larger.

To make a complete collection of our theoretical results, we present the centrality dependence and the  $n$  dependence of the flow harmonics  $v_n$  of dileptons in the following.

In Fig.10 is shown the elliptic flow of thermal dielectrons from AuAu collisions at  $\sqrt{s_{NN}} = 200$  GeV for different centralities: 0-10% (pink dashed line), 10-40% (red dotted line), 40-80% (dark blue dashed-dotted line). The centrality dependence of high order  $n$  is also investigated. A strong centrality dependence, from central to peripheral collisions, occurs not only to the elliptic flow but also to higher order,  $n = 3, 4, 5$ .

In Fig.11, the higher order harmonics coefficients  $v_n$  ( $n = 2, 3, 4, 5$ ) of thermal dielectrons from Au-Au collisions at  $\sqrt{s_{NN}} = 200$  GeV with centrality of 10-40% is presented. The curves have same shape, same trend as direct photons. The magnitude decreases monotonically with the order  $n$ . And it is the case for all the investigated centrality class, 0-10%, 10-40% and 40-80%. The low  $pt$  charged hadrons behaves similarly, as observed by ALICE [39].

It's often said that the development of anisotropic flow is controlled by the anisotropies in the pressure gradients which in turn depend on the shape and structure of the initial density profile. The latter can be characterized by a set of harmonic eccentricity coefficients  $\epsilon_n$  as defined in [40]. The initial space eccentricity  $\epsilon_n$  as a function of centrality for  $n = 2, 3, 4, 5$  in EPOS3 is shown in Fig.12, which looks quite similar to the initial space eccentricity in IP-Glasma, MC-Glauber and MC-KLN as shown in [40].



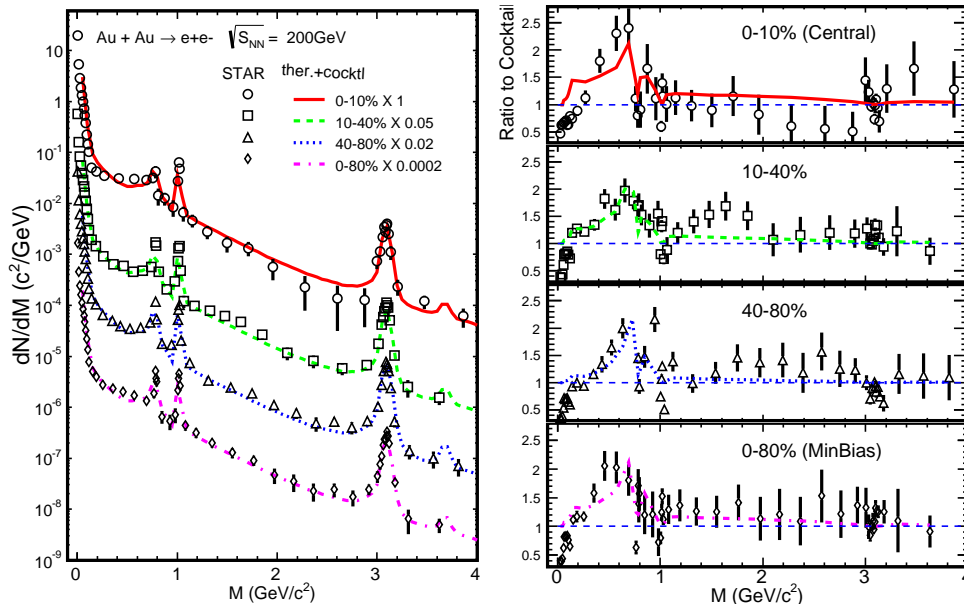


Figure 8: (Color Online) Left panel: Invariant mass spectra of dielectrons from EPOS3+DiL1 compared to STAR data [2, 37], for centrality 0-10% (central), 10-40%, 40-80%, 0-80% (MinBias) (from top to bottom). Right panel: Ratios of STAR dilepton invariant mass spectra and our calculations to cocktail, for centrality 0-10% (central), 10-40%, 40-80%, 0-80% (MinBias) (from top to bottom).

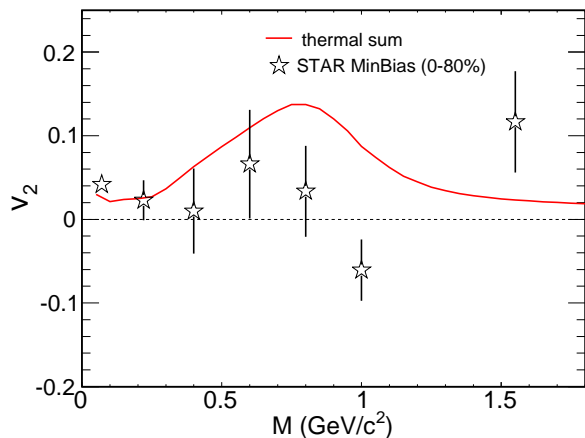


Figure 9: (Color Online) Thermal elliptic flow of dielectrons from  $\sqrt{s_{NN}} = 200$  GeV Au+Au minimum bias collisions and comparison with STAR data [38].

What builds up such a large elliptic flow of thermal dileptons, as shown in Fig. 9? The same question is asked in the direct photons paper based on EPOS3 [20].

As explained there, most models predict an elliptic flow too low, whereas EPOS3 can reproduce the measured elliptic flow. A systematic study [20] on the time evolution of space eccentricity and momentum eccentricity of the hot dense matter in EPOS3 shows that a correct interplay between the momentum eccentricity and radial flow is important to account for the elliptic flow of both hadrons and electromagnetic probes, dileptons and direct photons. Compared to the surface emission of hadrons, the overall emission inside the hot dense matter makes direct photons and dileptons more sensitive to the radial flow. Thus a large elliptic flow of direct photons and dileptons are obtained at the same time, with a larger mean radial flow and smaller momentum eccentricity. It should be said that we use the default EPOS3, with all parameters fixed from hadronic observables.

#### IV. DISCUSSION AND CONCLUSION

We investigated the anisotropic emission of thermal dileptons from Au+Au central collision at  $\sqrt{s_{NN}} = 200$  GeV at the RHIC, accompanying the study of the direct photons in [20], where a possible solution to the direct photon puzzle is provided.

With a detailed explanation of dilepton emission rate



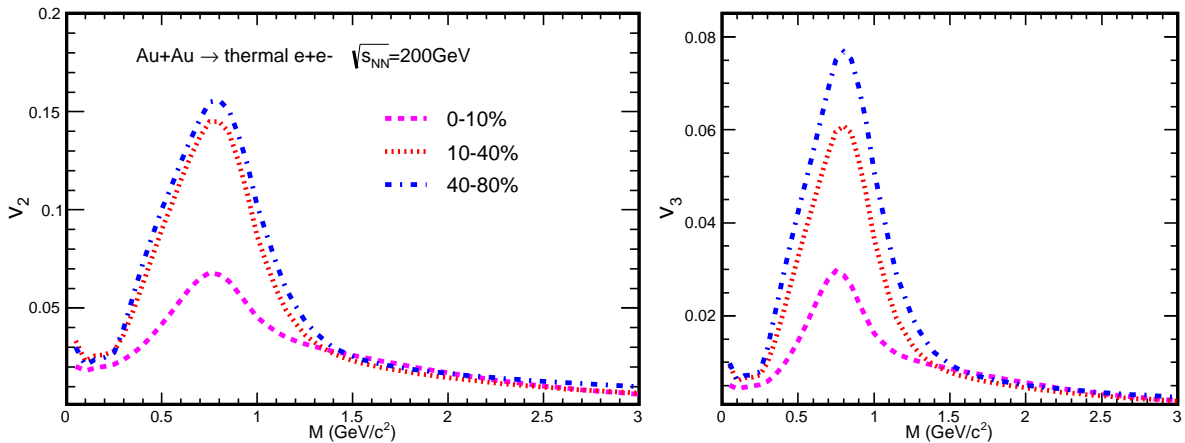


Figure 10: (Color Online) The elliptic flow (left) and trianger flow (right) of thermal dielectrons from AuAu collisions at  $\sqrt{s_{NN}} = 200$  GeV. 0-10%(pink dashed line), 10-40%(red dotted line), 40-80%(dark blue dashed-dotted line).

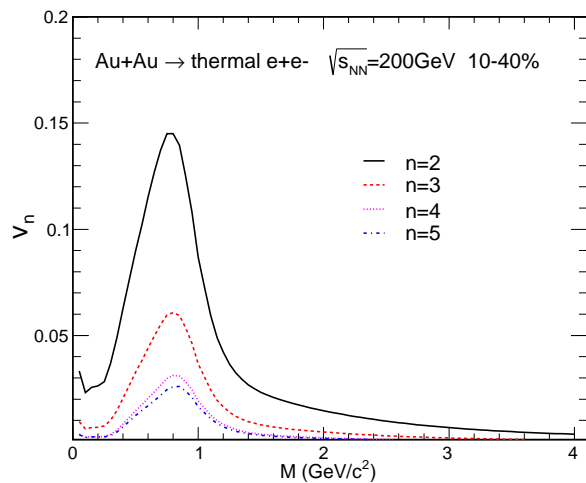


Figure 11: (Color Online) Predicated harmonics coefficients  $v_n$  ( $n = 2, 3, 4, 5$ ) of thermal dielectrons are shown by various curves for centrality 10-40%.

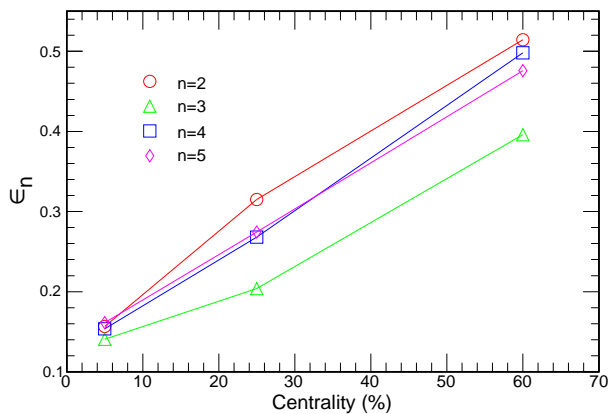


Figure 12: (Color Online) Eccentricity  $e_n$  as function of centrality for  $n = 2, 3, 4, 5$  with EPOS3.

and a relatively brief explanation of the space-time evolution within EPOS3, we first calculated the thermal contribution (from QGP and  $\rho$  mesons) to the invariant mass spectra at different centralities, comparing with the cocktail contribution. The thermal contribution does play an important role in the low invariant mass region, ie,  $M < 1\text{GeV}/c^2$ , which offers a useful window to study the hot and dense matter created in relativistic heavy ion collisions, especially the early stage of the hot and dense matter. Our calculated spectra, together with STAR cocktail, could reasonable well reproduce STAR's measured invariant mass spectra of di-electron at different centralities.

Then, we investigated elliptic flow and higher order harmonics of thermal dileptons. The elliptic flow of thermal dileptons is predicted to be quite large, larger than in other models, and comparable to the dilepton data for centrality 0-80%.

Finally, we made predictions of the  $v_n$  of thermal dileptons for  $2 \leq n \leq 5$  at three centrality classes, 0-10%, 10-40%, and 40-80%. The  $v_n$  of thermal dileptons is found to decrease with  $n$  monotonically for the three centrality class. The same centrality dependence for  $2 \leq n \leq 5$  is observed with EPOS3, namely, more central collisions provide smaller  $v_n$  of thermal dileptons. Further experimental measurements are highly awaited to test our solution to the puzzle of direct photon elliptic flow and improve our understanding of the created hot and dense matter.

## Acknowledgments

S. X. Liu thanks J. Zhao and H. J. Xu for very helpful discussion. This work was supported by the Natural Science Foundation of China under Project No.11275081 and by the Program for New Century Excellent Talents

in University (NCET).

- 
- [1] A. Adare *et al.* (PHENIX Collaboration), Phys. Rev. C **81**, 034911 (2010).
- [2] L. Adamczyk *et al.* (STAR Collaboration), Phys. Rev. Lett **113**, 022301 (2014).
- [3] E. Shuryak, Phys. Lett. B **78** (1978) 150.
- [4] D. Adamova *et al.*, Phys. Lett. B **666** (2008) 425.
- [5] G. Agakichiev *et al.* Eur. Phys. J. C **41** (2005) 475.
- [6] R. Arnaldi *et al.* Eur. Phys. J. **59** (2009) 607.
- [7] R. Rapp and J. Wambach, Adv. Nucl. Phys. **25** (2000) 1.
- [8] R. Rapp, Phys. Rev. C **63**, 054907 (2001).
- [9] R. Rapp, Adv.High Energy Phys. **2013** (2013) 148253, arXiv:1304.2309.
- [10] V. L. Eletsky, M. Belkacem, P. J. Ellis, and J. I. Kapusta, Phys. Rev. C **64**, 035202 (2001).
- [11] G. Vujanovic, C. Young, B. Schenke, R. Rapp, S. J. Jeon and C. Gale, Phys. Rev. C **89** (2014) 034904.
- [12] R. Rapp, J. Phys. G **34**, S405 (2007).
- [13] Hao-jie Xu, Hong-fang Chen, Xin Dong, Qun Wang, and Yi-fei Zhang, Phys. Rev. C **85**, 024906 (2012).
- [14] O. Linnyk *et al.*, Phys. Rev. C **84**, 054917 (2011).
- [15] O. Linnyk *et al.*, Phys. Rev. C **85**, 024910 (2012).
- [16] W. Cassing and E. L. Bratkovskaya, Nucl. Phys. A **831**, 215 (2009); E. L. Bratkovskaya, W. Cassing, V. P. Konchakovski, and O. Linnyk, Nucl. Phys. A **856**, 162 (2011).
- [17] R. Chatterjee, D. K. Srivastava, U. W. Heinz and C. Gale, Phys. Rev. C **75**, 054909 (2007)
- [18] P. Mohanty, V. Roy, S. Ghosh, S. K. Das, B. Mohanty, S. Sarkar, J.-e Alam and A. K. Chaudhuri, Phys. Rev. C **85**, 031903 (2012).
- [19] Hao-Jie Xu, Longgang Pang, Qun Wang, Phys. Rev. C **89**(2014) 064902.
- [20] Fu-Ming Liu, Sheng-Xu Liu, Klaus Werner, [nucl-th, hep-ph].
- [21] K. Werner, B. Guiot, Iu. Karpenko, T. Pierog, arXiv:1312.1233 [nucl-th]. Published in Phys.Rev. C89 (2014) 6, 064903.
- [22] L. Adamczyk *et al.* (STAR Collaboration) Phys. Rev. C **86** (2012) 024906.
- [23] H.J. Drescher, M. Hladik, S. Ostapchenko, T. Pierog, K. Werner, Phys.Rept. 350 (2001) 93-289.
- [24] K. Werner, Iu. Karpenko, T. Pierog, M. Bleicher, K. Mikhailov, Phys.Rev. C82 (2010) 044904.
- [25] Klaus Werner, Phys.Rev.Lett. 98 (2007) 152301.
- [26] M. Bleicher *et al.*, J. Phys. G25 (1999) 1859; H. Petersen, J. Steinheimer, G. Burau, M. Bleicher and H. Stocker, Phys. Rev. C78 (2008) 044901
- [27] K. Werner, I. Karpenko, T. Pierog, M. Bleicher and K. Mikhailov, Phys. Rev. C **82**, 044904 (2010) doi:10.1103/PhysRevC.82.044904 [arXiv:1004.0805 [nucl-th]].
- [28] H. T. Ding, A. Francis, O. Kaczmarek, F. Karsch, E. Laermann and W. Soeldner, Phys. Rev. D **83**, 034504 (2011).
- [29] G. J. Gounaris and J. J. Sakurai, Phys. Rev. Lett. **21**, 244 (Jul 1968).
- [30] C. Gale and J. I. Kapusta, Nucl. Phys. **B357**, 65 (1991).
- [31] R. F. Schwitters and K. Strauch, Annu. Rev. Nucl. Sci. **26**, 89 (1976).
- [32] R. Rapp, Phys. Rev. C **60**, 024903 (1999).
- [33] G. Vujanovic, C. Young, B. Schenke, S. Jeon, R. Rapp and C. Gale, Nucl. Phys. A **904-905**, 557c (2013) [arXiv:1211.0022 [hep-ph]].
- [34] C. Shen, U. W. Heinz, J. F. Paquet and C. Gale, Phys. Rev. C **89**, no. 4, 044910 (2014) [arXiv:1308.2440 [nucl-th]].
- [35] Fu-Ming Liu, and Sheng-Xu Liu, Phys. Rev. C **89** (2014) 034906.
- [36] C. Gale, S. Jeon, B. Schenke, P. Tribedy and R. Venugopalan, Phys. Rev. Lett. **110**, no. 1, 012302 (2013) [arXiv:1209.6330 [nucl-th]].
- [37] L. Adamczyk *et al.* (STAR Collaboration) (2015) arXiv:1504.01317.
- [38] L. Adamczyk *et al.* (STAR Collaboration) Phys. Rev. C **90** (2014) 64904.
- [39] K. Aamodt *et al.* [ALICE Collaboration], Phys. Rev. Lett. **107**, 032301 (2011) [arXiv:1105.3865 [nucl-ex]].
- [40] U. Heinz and R. Snellings, Ann. Rev. Nucl. Part. Sci. **63** (2013) 123 [arXiv:1301.2826 [nucl-th]].